大阪公立大学
Osaka Metropolitan University
学術情報リポジトリ

Analysis of a dc bus system with a nonlinear constant power load and its delayed feedback control

メタデータ	言語: eng 出版者: 公開日: 2020-09-11 キーワード (Ja): キーワード (En): 作成者: Konishi, Keiji, Sugitani, Yoshiki, Hara, Naoyuki メールアドレス: 所属:
URL	http://hdl.handle.net/10466/00017034

Analysis of a dc bus system with a nonlinear constant power load and its delayed feedback control

Keiji Konishi,* Yoshiki Sugitani, and Naoyuki Hara
Department of Electrical and Information Systems, Osaka Prefecture University and 1-1 Gakuen-cho, Naka-ku, Sakai, Osaka 599-8531, Japan
(Received 10 November 2013; published 7 February 2014)

This paper tackles a destabilizing problem of a direct-current (dc) bus system with constant power loads, which can be considered a fundamental problem of dc power grid networks. The present paper clarifies scenarios of the destabilization and applies the well-known delayed-feedback control to the stabilization of the destabilized bus system on the basis of nonlinear science. Further, we propose a systematic procedure for designing the delayed feedback controller. This controller can converge the bus voltage exactly on an unstable operating point without accurate information and can track it using tiny control energy even when a system parameter, such as the power consumption of the load, is slowly varied. These features demonstrate that delayed feedback control can be considered a strong candidate for solving the destabilizing problem.

DOI: 10.1103/PhysRevE.89.022906 PACS number(s): 05.45.Xt, 05.45.Ra, 05.45.Gg, 89.75.−k

I. INTRODUCTION

The dynamics of power-grid networks has attracted considerable attention in the field of nonlinear science (see Refs. [1,2] and references therein). Most of these studies investigate the dynamics of the alternating-current (ac) power-grid networks which are widely used in daily life. On the other hand, it is well accepted in the field of power electronics that direct-current (dc) bus systems will play an important role in future power systems [3] (see Fig. 1). The main reasons are as follows: power sources are easy to integrate due to phase control being unnecessary; renewable and alternative power sources typically generate dc electric power; and the utilization of dc loads in electronics, such as information technology equipment, is increasing at a rapid rate [3,4].

Many types of dc loads employ a point-of-load power conditioning and control system. Such loads behave as constant power loads (CPLs), which consume a constant power independent of their supply voltage; they can be regarded as nonlinear negative resistances, since the input current decreases (increases) with an increase (decrease) of the supply voltage [5]. Such negative resistances can induce *destabilization* of dc voltages. This is a crucial problem for dc bus systems in practical use. Very recently, there have been various studies on analyzing and solving this problem in the field of power electronics. The destabilizing phenomenon has been investigated from various viewpoints: dynamical behavior and basin of an operating point [6], linear stability of the operating point [7], basin of the operating point with multistage filters [8], and dynamics of a discrete-time model [9]. Further, several strategies for enhancing the stability of an operating point have been demonstrated as follows: use of passive damping [5], application of a bidirectional dc-dc converter [10], use of a virtual capacitor [11], feedback control based on the vector field [3,12], and control for multiple power sources and loads [13–16].

These studies have tackled the destabilization problem from viewpoint of power electronics. However, for this problem, there has been little study on analysis and control based on nonlinear science. The present paper thoroughly investigates the nonlinear dynamics of a simplified dc bus system on the basis of bifurcation theory [17]. Further, a delayed feedback control [18,19], one of the most popular methods for stabilizing unstable periodic orbits [20,21] and unstable fixed points [22–27] in nonlinear systems, is introduced to solve the destabilization problem. This is because the delayed feedback control has the following advantages: A system state converges exactly on an unstable fixed point with its noninvasive property [28], even though the location of the point is unknown and the state can track a wandering point using tiny control energy when a system parameter is slowly varied. The analytical results based on bifurcation theory allow us to provide a systematic procedure for designing a controller. Some numerical examples demonstrate that the designed controller works well for the stabilization of a destabilized operating point.

The following notation is used in this paper. The principal argument of a complex number z is denoted by $\mathrm{Arg}[\mathsf{z}] \in [0,2\pi)$. For a real number x, the largest integer that is not greater than x is denoted by $\lfloor \mathsf{x} \rfloor$.

II. SIMPLIFIED DC BUS SYSTEM

Consider the simplified dc bus system shown in Fig. 2, in which E, r, L, and C represent the dc voltage source, the equivalent resistance, the inductance, and the capacitance of the dc bus, respectively. The dc bus voltage, denoted by $v_{\mathrm{P}}(t)$, is applied to a CPL. The currents $i_{\mathrm{L}}(t)$ and $i_{\mathrm{P}}(t)$ are through the L and CPL, respectively. The product of $v_{\mathrm{P}}(t)$ and $i_{\mathrm{P}}(t)$ in the CPL is always constant P: $v_{\mathrm{P}}(t)i_{\mathrm{P}}(t) = P$, $\forall t \geqslant 0$. We can model the circuit illustrated in Fig. 2 by

$$\begin{aligned} C\frac{dv_{\mathrm{P}}(t)}{dt} &= -\frac{P}{v_{\mathrm{P}}(t)} + i_{\mathrm{L}}(t), \\ L\frac{di_{\mathrm{L}}(t)}{dt} &= -v_{\mathrm{P}}(t) - ri_{\mathrm{L}}(t) + E. \end{aligned} \tag{1}$$

The dynamics of Eq. (1) depend on the *five* circuit parameters r, L, C, P, and E. One of the main purposes of this paper is to clarify how these parameters influence the circuit dynamics. To that end, transformation of the system states and time,

$$x := \frac{1}{E}v_{\mathrm{P}}, \quad y := \frac{L}{rCE}i_{\mathrm{L}}, \quad \tau := \frac{t}{rC},$$

*http://www.eis.osakafu-u.ac.jp/~ecs

 ©2014 American Physical Society

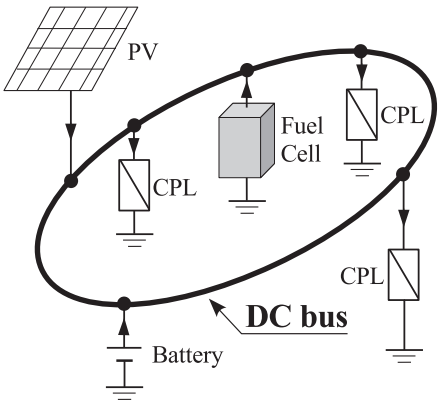

FIG. 1. Conceptual diagram of a dc bus system (CPL: constant power load; PV: photovoltaic cell).

and the parameters,

$$a := \frac{rP}{E^2}, \quad b := \frac{r^2}{L/C}, \tag{2}$$

are applied to Eq. (1). We can then write a simple dimensionless model for the circuit as

$$\dot{x} = -\frac{a}{x} + by, \quad \dot{y} = -x - by + 1, \tag{3}$$

where $\dot{x}$ denotes the derivative of x with respect to the dimensionless time τ. Notice that parameters (2) have the following properties:

a: Proportional to the power of the CPL, P, and resistance r and inversely proportional to the square of voltage source E;

b: Proportional to the square of resistance r and inversely proportional to L/C.

Since system (3) has only the *two* dimensionless parameters $a > 0$ and $b > 0$, we can analytically clarify the influence of these parameters on the circuit dynamics. This paper will deal with dimensionless dynamical system (3) for analysis and its control instead of circuit (1).

III. BIFURCATION ANALYSIS

This section will investigate the dynamics of system (3) on the basis of bifurcation theory.

A. Analytical results

The fixed points $\boldsymbol{p}_+ := [x_+^*, y_+^*]^T$ and $\boldsymbol{p}_- := [x_-^*, y_-^*]^T$, where

$$x_\pm^* = \frac{1}{2}(1 \pm \sqrt{1-4a}), \quad y_\pm^* = \frac{a}{bx_\pm^*}, \tag{4}$$

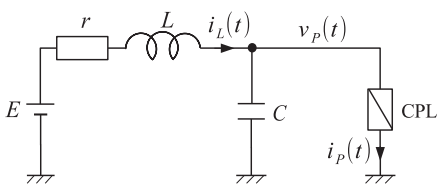

FIG. 2. Simplified dc bus system.

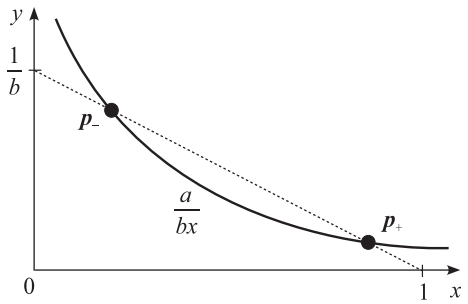

FIG. 3. Nullclines of system (3) (bold line: $\dot{x} = 0$; dotted line: $\dot{y} = 0$).

are located at the intersections of the nullclines of system (3) as sketched in Fig. 3. $\boldsymbol{p}_\pm$ correspond to the operating points of circuit (1). Figure 3 suggests that $\boldsymbol{p}_\pm$ are born and die via the saddle-node (SN) bifurcation. Here we consider the stability of $\boldsymbol{p}_\pm$, which is governed by the characteristic equation at $\boldsymbol{p}_\pm$,

$$f(s, x_\pm^*) = 0, \tag{5}$$

where

$$f(s,x) := s^2 + \left(b - \frac{a}{x^2}\right)s + b - \frac{ab}{x^2}. \tag{6}$$

Now we find a *double-zero* (DZ) bifurcation point [17], where Eq. (5) has double roots at $s = 0$.

Lemma 1. A double-zero bifurcation occurs in dimensionless system (3) at

$$4a = 1, \quad b = 1. \tag{7}$$

Proof. Equation (5) has double roots at $s = 0$ when its coefficients for s^1 and s^0 are zero. It is easy to find condition (7) from Eq. (6) with Eq. (4). ■

Here we find an existence condition for SN bifurcation and that for the fixed points.

Lemma 2. Consider dimensionless system (3). SN bifurcation occurs at

$$a = \tfrac{1}{4}, \tag{8}$$

with the exception of DZ bifurcation point (7). Further, there exist

$$\boldsymbol{p}_\pm \in \{(x,y) : 0 < x < 1,\ 0 < y < 1/b\}$$

for $a < 1/4$, but not for $a > 1/4$.

Proof. We omit this proof, since it is straightforward to find this condition from Eqs. (4) and (6). ■

Further, we show an existence condition for Hopf (HP) bifurcation and find its bifurcation curve.

Lemma 3. Consider dimensionless system (3) which has the fixed points $\boldsymbol{p}_\pm$. HP bifurcation at $\boldsymbol{p}_+$ can occur on

$$a = \frac{b}{(1+b)^2} \tag{9}$$

if and only if $b < 1$ holds. On the other hand, HP bifurcation never occurs at $\boldsymbol{p}_-$.

Proof. See Appendix A 1. ■

Now we will seek a condition for when the type of fixed points changes from focus to node. This change occurs when the locus of two different real roots coalesces and then departs

from the real axis in the complex plane. In the field of control theory, the point on the real axis at which this change occurs is called the *breakaway* point [29]. Here we introduce an existence condition for breakaway and its bifurcation curve.

Lemma 4. Consider dimensionless system (3) which has the fixed points $\boldsymbol{p}_{\pm}$. The type of $\boldsymbol{p}_{+}$ changes from focus to node (i.e., breakaway occurs) when

$$a = \frac{2\sqrt{b} - b}{(1 + 2\sqrt{b} - b)^2} \tag{10}$$

if and only if $b < 4$ holds with the exception of DZ bifurcation point (7). Such a change never occurs at $\boldsymbol{p}_{-}$.

Proof. See Appendix A 2. ■

These analytical results provide us with useful information for understanding the dynamical behavior of system (3). The following section will show a numerical example based on such analytical information.

B. Numerical example

We will investigate how the parameters a and b influence the dynamics of system (3). Figures 4(a) and 4(b) show the bifurcation curves for $\boldsymbol{p}_{+}$ and $\boldsymbol{p}_{-}$, respectively. The DZ bifurcation point in Lemma 1 is represented by an open square. The SN bifurcation lines estimated by Eq. (8) in Lemma 2 suggest that there exist $\boldsymbol{p}_{\pm}$ under the lines. In addition, Lemma 3 indicates that the HP bifurcation curve for $\boldsymbol{p}_{+}$, estimated by Eq. (9), exists for $b < 1$. Lemma 4 provides the information that the breakaway of $\boldsymbol{p}_{+}$ occurs on the broken curve given by

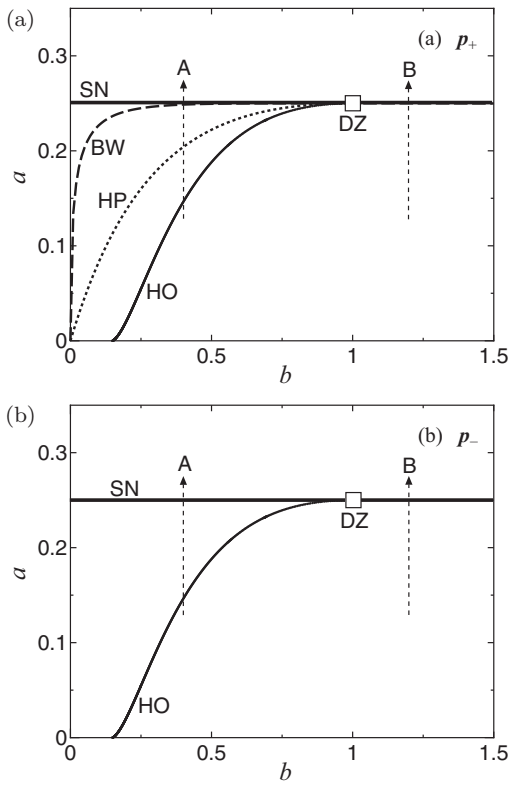

FIG. 4. Bifurcation curves of system (3): (a) $\boldsymbol{p}_{+}$ and (b) $\boldsymbol{p}_{-}$. SN: saddle-node bifurcation; HP: Hopf bifurcation; HO: Homoclinic bifurcation; DZ: double-zero bifurcation; BW: breakaway.

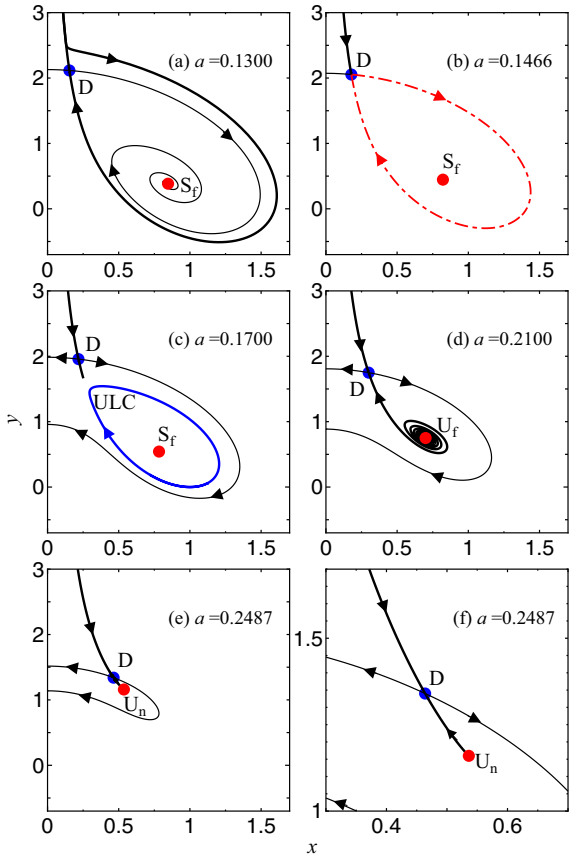

FIG. 5. (Color online) Phase portraits of system (3) ($b = 0.40$). These portraits correspond to the arrowed broken line A in Fig. 4. D: saddle; S_f: stable focus; U_f: unstable focus; U_n: unstable node; ULC: unstable limit cycle.

Eq. (10) in the range $b \in (0,4)$ with the exception of the DZ bifurcation point $b = 1$.

The homoclinic (HO) bifurcation, a typical global bifurcation, is estimated by the bifurcation tool MATCONT [30]. It can be seen that the HO bifurcation curves exist for $b < 1$ and coalesce with the HP bifurcation curve at the DZ bifurcation point.

Figure 5 shows the phase portraits (x versus y) at $b = 0.40$ and $a \in [0.1300, 0.2487]$, which correspond to the arrowed broken line A in Fig. 4. As shown in Fig. 5(a), for $a = 0.1300$, $\boldsymbol{p}_{-}$ is the saddle point (D) and $\boldsymbol{p}_{+}$ is the stable focus (S_f), and the ω branch of D is the basin boundary of S_f [31]. The α and ω branches of D move closer together with an increase of a; eventually, they link together (i.e., HO bifurcation) at $a = 0.1466$ as illustrated in Fig. 5(b). This linked branch described by the dashed-dotted curve is the homoclinic orbit. A further increase of a induces an unstable limit cycle (ULC), the basin boundary of S_f, from the homoclinic orbit [see Fig. 5(c)]. ULC becomes smaller with an increase of a; ultimately, ULC and S_f coalesce. Then S_f changes to an unstable focus (U_f) and ULC disappears, as shown in Fig. 5(d). This is the subcritical HP bifurcation. After this bifurcation, there is no stable steady state. This situation corresponds to that of the dc bus system of Fig. 2, whereby dc power cannot be provided to the CPL. The type of $\boldsymbol{p}_{+}$ is changed from an unstable focus to an unstable

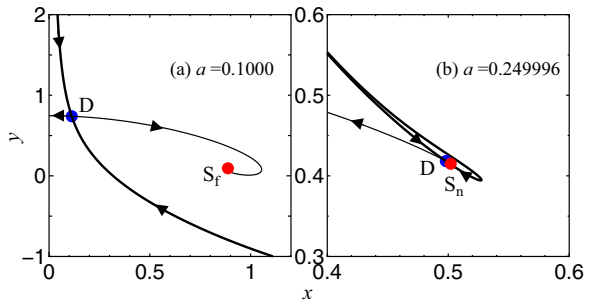

FIG. 6. (Color online) Phase portraits of system (3) ($b = 1.20$). These portraits correspond to the arrowed broken line B in Fig. 4. S_n: stable node.

node (i.e., breakaway) by a further increase of a. Figure 5(e) and its enlarged view [Fig. 5(f)] show that the saddle (D) and the unstable node (U_n) have a common branch. A further increase of a induces the SN bifurcation where they coalesce and disappear.

Figure 6 shows the phase portraits at $b = 1.20$ and $a \in \{0.1000, 0.249996\}$, which correspond to the arrowed broken line B in Fig. 4. For $a = 0.1000$, $\boldsymbol{p}_-$ is the saddle (D) and $\boldsymbol{p}_+$ is the stable focus (S_f), as illustrated in Fig. 6(a). The ω branch of D is the basin boundary of S_f. The type of $\boldsymbol{p}_+$ changes from a stable focus to a stable node (S_n) by a further increase of a [see Fig. 6(b)]. The saddle and node eventually coalesce and disappear via the SN bifurcation.

From the viewpoint of circuit parameters, we summarize our bifurcation analysis for the two situations: $b < 1 \Leftrightarrow r < \sqrt{L/C}$ (see Fig. 5) and $b > 1 \Leftrightarrow r > \sqrt{L/C}$ (see Fig. 6). An increase of $a = rP/E^2$ induces the following scenarios:

(1) $r < \sqrt{L/C}$: The operating point $\boldsymbol{p}_+$ changes from a stable focus to an unstable focus via a Hopf bifurcation, from an unstable focus to an unstable node via a breakaway, and finally disappears via a saddle-node bifurcation.

(2) $r > \sqrt{L/C}$: The operating point $\boldsymbol{p}_+$ changes from a stable focus to a stable node via a breakaway and finally disappears via a saddle-node bifurcation.

It can be seen that the bifurcation scenario of the operating point $\boldsymbol{p}_+$ strongly depends on the balance between r and $\sqrt{L/C}$.

IV. DELAYED FEEDBACK CONTROL OF A DC BUS SYSTEM

This section will show that an unstable operating point $\boldsymbol{p}_+$ can be stabilized by the well-known delayed feedback control. A systematic procedure for designing the controller will be provided on the basis of our previous result [23] in the field of control theory. A numerical example will demonstrate that the designed controller works well and that it can track the stabilized point even when the power consumption of the load (i.e., parameter a) is slowly varied.

A. Control system

A delayed feedback controller is added to the simplified dc bus system, as illustrated in Fig. 7. We can write the circuit

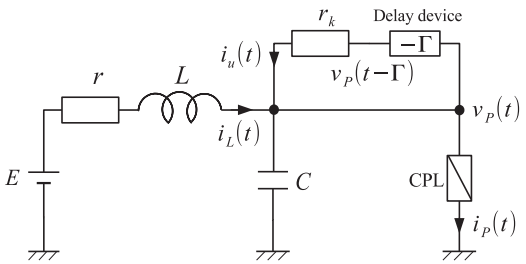

FIG. 7. Simplified dc bus system with delayed feedback control.

equation as

$$C\frac{dv_{\mathrm{P}}(t)}{dt} = -\frac{P}{v_{\mathrm{P}}(t)} + i_{\mathrm{L}}(t) + i_u(t),$$
$$L\frac{di_{\mathrm{L}}(t)}{dt} = -v_{\mathrm{P}}(t) - ri_{\mathrm{L}}(t) + E,$$

where $i_u(t)$ represents the current injected from the controller, that is,

$$i_u(t) = \frac{1}{r_k}\left\{v_{\mathrm{P}}(t-\Gamma) - v_{\mathrm{P}}(t)\right\}.$$

Note that $v_{\mathrm{P}}(t-\Gamma)$ denotes the past bus voltage with delay time Γ. Transformation of variables and parameters,

$$x_T := \frac{1}{E}v_{\mathrm{P}}(t-\Gamma), \quad T := \frac{\Gamma}{rC}, \quad k := \frac{r}{r_k},$$

allows us to obtain a dimensionless dynamical system,

$$\dot{x} = -\frac{a}{x} + by + u, \quad \dot{y} = -x - by + 1, \tag{11}$$

with delayed feedback control,

$$u = k\,(x_T - x)\,. \tag{12}$$

It should be noted that the analytical approach in the preceding section cannot be used for dynamical system (11) with controller (12) due to its infinite dimension. Also note that the location of $\boldsymbol{p}_\pm$ in system (11) without control [i.e., system (3)] never moves, even for system (11) with control.

Since the operating point always corresponds to $\boldsymbol{p}_+$, as analytically shown in Sec. III, we will focus only on the stability of $\boldsymbol{p}_+$ in the controlled dynamical system. The linearized system with control at $\boldsymbol{p}_+$ is described by

$$\begin{bmatrix}\dot{x}_\Delta \\ \dot{y}_\Delta\end{bmatrix} = \begin{bmatrix}-k + a/(x_+^*)^2 & b \\ -1 & -b\end{bmatrix}\begin{bmatrix}x_\Delta \\ y_\Delta\end{bmatrix} + \begin{bmatrix}k & 0 \\ 0 & 0\end{bmatrix}\begin{bmatrix}x_{\Delta T} \\ y_{\Delta T}\end{bmatrix}, \tag{13}$$

where $x_\Delta := x - x_+^*$, $y_\Delta := y - y_+^*$, $x_{\Delta T} := x_T - x_+^*$, and $y_{\Delta T} := y_T - y_+^*$. The stability of linear system (13) is governed by its characteristic quasipolynomial,

$$g(s,T) := s^2 + \gamma_1 s + \gamma_2 + (\eta_1 s + \eta_2)(1 - e^{-sT}), \tag{14}$$

where its coefficients are

$$\gamma_1 := b - \frac{a}{(x_+^*)^2}, \quad \gamma_2 := b - \frac{ab}{(x_+^*)^2},$$
$$\eta_1 := k, \quad \eta_2 := kb. \tag{15}$$

From Eq. (6), we notice that the first three terms of Eq. (14), which are identical to $g(s,0)$, govern the stability of $\boldsymbol{p}_+$ in system (3). The fourth term depends on controller (12). Recall that $\boldsymbol{p}_+$ is stable if and only if the infinite number of roots for $g(s,T)=0$ are all in the open left half plane.

B. Stability analysis

The main purpose of this section is to propose a systematic procedure for designing the controller parameter k and T such that $\boldsymbol{p}_+$ is stable. Let us review a key result given by Kokame *et al.* [23] in preparation for our proposal.

Theorem 1 (Ref. [23]). Consider the stability of the characteristic quasipolynomial

$$g(s,T)=s^2+\gamma_1 s+\gamma_2+(\eta_1 s+\eta_2)(1-e^{-sT}) \tag{16}$$

under the assumption

$$\gamma_1<0,\ \gamma_2>0. \tag{17}$$

If the coefficients of Eq. (16), $\gamma_{1,2}$ and $\eta_{1,2}$, satisfy the four inequalities

$$\begin{aligned} d_0&:=\gamma_2+2\eta_2>0,\\ d_1&:=\gamma_1^2+2(\gamma_1\eta_1-\gamma_2-\eta_2)<0,\\ d_2&:=d_1^2-4\left(\gamma_2^2+2\gamma_2\eta_2\right)>0,\\ d_3&:=\frac{\psi_1}{\omega_1}-\frac{\psi_2}{\omega_2}<0, \end{aligned} \tag{18}$$

where

$$\begin{aligned} \omega_1&:=\sqrt{\frac{-d_1-\sqrt{d_2}}{2}},\quad \omega_2:=\sqrt{\frac{-d_1+\sqrt{d_2}}{2}},\\ \psi_i&:=\mathrm{Arg}\frac{\eta_2+j\omega_i\eta_1}{\gamma_2+\eta_2-\omega_i^2+j\omega_i(\gamma_1+\eta_1)},\\ i&=1,2, \end{aligned} \tag{19}$$

then there exists T such that $g(s,T)$ is stable. Further, under condition (18), $g(s,T)$ is stable if and only if T belongs to one of the intervals

$$\begin{aligned} T&\in\left(\frac{\psi_1+2\pi l}{\omega_1},\frac{\psi_2+2\pi l}{\omega_2}\right),\\ l&=0,\ldots,\left\lfloor\frac{\psi_2\omega_1-\psi_1\omega_2}{2\pi(\omega_2-\omega_1)}\right\rfloor. \end{aligned} \tag{20}$$

As Eq. (16) in this theorem is equivalent to our characteristic quasipolynomial (14), we can associate assumption (17) with the following facts: $\gamma_1<0$ is a necessary condition for the characteristic function at $\boldsymbol{p}_+$ without control, $g(s,0)$, to be unstable; and for $\gamma_2<0$, which contradicts assumption (17), the fixed point $\boldsymbol{p}_+$ cannot be stabilized, since $g(s,0)=0$ has a positive and a negative real root (i.e., the well-known odd-number limitation [32]). These facts suggest that $g(s,0)=0$ with assumption (17) has its two roots in the open right half plane. The following corollary clarifies system (3) under assumption (17).

Corollary 1. Assumption (17) for system (3) is given by

$$a\in\left(\frac{b}{(1+b)^2},\frac{1}{4}\right),\quad b<1. \tag{21}$$

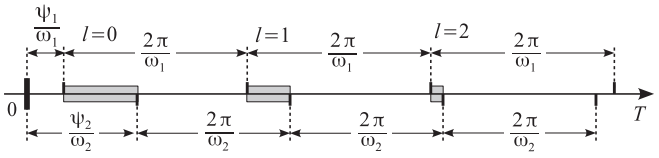

FIG. 8. Sketch of $\psi_{1,2},\omega_{1,2},T$ introduced in Theorem 1: $g(s,T)$ is stable within the gray intervals.

Proof. As it is easy to derive assumption (21) from $\gamma_{1,2}$ in Eq. (15) and x_+^* in Eq. (4), this proof is omitted. ■

The relationships between $\psi_{1,2}$, $\omega_{1,2}$, and T introduced in Theorem 1 are sketched in Fig. 8. Assumption (17) guarantees that $g(s,T)=0$ with $T=0$ has two unstable roots. For $T>0$, we know that $g(s,T)=0$ has an infinite number of roots. Increasing T from 0, the pair of dominant complex-conjugate roots moves from the right to the left at $T=\psi_1/\omega_1$. Thus, $g(s,T)$ becomes stable. A further increase of T moves the pair of dominant complex-conjugate roots from the left to the right at $T=\psi_2/\omega_2$; from here, $g(s,T)$ becomes unstable. This movement from the right to the left (the left to the right) is repeated with period $2\pi/\omega_1$ ($2\pi/\omega_2$). The gray intervals in Fig. 8 represent the stable intervals of $g(s,T)$. From Eq. (19), we notice that $\omega_1<\omega_2$ holds; then we have $2\pi/\omega_1>2\pi/\omega_2$. This guarantees that the intervals narrow with an increase in T and eventually disappear.

We will estimate a stabilizable parameter space (b versus a) where there exists T such that $g(s,T)$ at $\boldsymbol{p}_+$ is stable. Figure 9(a) illustrates the HP and SN bifurcation curves for $\boldsymbol{p}_+$ without control. Corollary 1 guarantees that assumption (17) holds only when b and a are within the parameter space between these curves. Now let us restrict our attention to the stability of $\boldsymbol{p}_+$ with control. The gray regions in Figs. 9(b), 9(c), and 9(d) are the stabilizable parameter spaces where inequalities (18) hold for $k=0.02$, 0.10, and 0.28, respectively. For instance, we focus on point A: $(b,a)=(0.20,0.17)$. Figures 9(b), 9(c), and 9(d) show that $\boldsymbol{p}_+$ is stabilized for

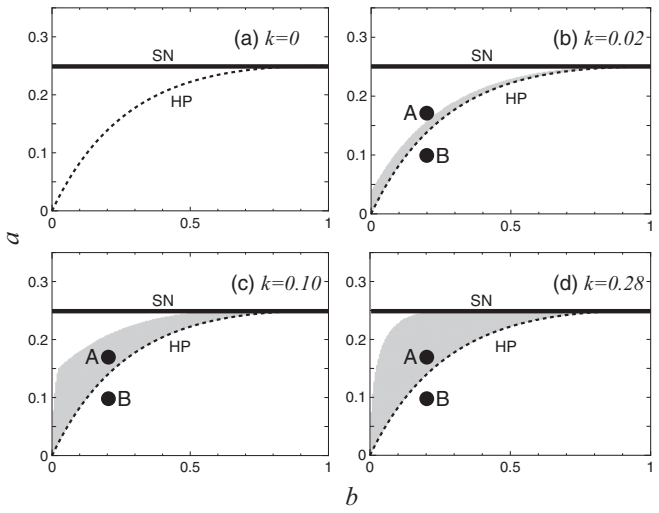

FIG. 9. Stabilizable parameter space. Inequalities (18) hold in the gray region.

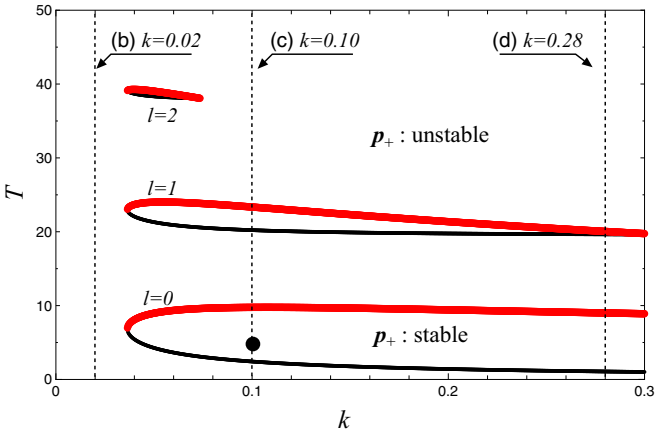

FIG. 10. (Color online) Stability regions in controller parameter space, k vs T ($a = 0.17$, $b = 0.20$). Thin black line: $(\psi_1 + 2\pi l)/\omega_1$; bold red line: $(\psi_2 + 2\pi l)/\omega_2$.

$k = 0.10, 0.28$, but not for $k = 0.02$. This suggests that the stabilizable parameter space depends on k.

C. Design of controller

The preceding subsection showed that, for a given k, the stabilizable parameter space can be estimated by inequalities (18). However, a design procedure for k is still lacking. This subsection proposes a systematic procedure for designing k and T such that $\boldsymbol{p}_+$ is stable for a given a and b.

Step 1: The parameters a and b are given.

Step 2: If these parameters satisfy Corollary 1, then go to the next step, otherwise we have to abandon our design.

Step 3: Substituting Eq. (15) with Eq. (4) into Eq. (18), $d_{0,1,2,3}$ are reduced to polynomials of only variable k. For k satisfying inequalities (18), the stable intervals of T are estimated from Eq. (20).

Let us design the controller in accordance with the above steps. (Step 1) The parameters $a = 0.17$ and $b = 0.20$ are given (see point A in Fig. 9). (Step 2) They satisfy Corollary 1, and so go to the next step. (Step 3) The polynomials $d_{0,1,2,3}$ with respect to variable k are derived. Figure 10 shows the stable intervals of T for positive values of k which satisfy inequalities (18). The thin black (bold red) curve of Fig. 10 denotes the critical T of which a pair of complex-conjugate roots moves from the right to the left (the left to the right) of the complex plane with an increase of T. The fixed point $\boldsymbol{p}_+$ is stable if and only if k and T are within the regions surrounded by these curves. We see that there are three stability regions for $l = 0, 1, 2$ in Eq. (20). Now we will clarify the relationship between these regions and the stabilizable parameter space shown in Fig. 9. The gains k used in Figs. 9(b), 9(c), and 9(d) are described by the dotted lines (b), (c), and (d) in Fig. 10, respectively. For (b) $k = 0.02$, as can be seen in Fig. 9(b), the point A is not within the stabilizable parameter space; thus, there does not exist T on the dotted line (b) in Fig. 10 within the stability regions. In contrast, for (c) $k = 0.10$, the point A is within the stabilizable parameter space [see Fig. 9(c)]. It can be seen that there exist T on the dotted line (c) in Fig. 10 within the stability regions. For (d) $k = 0.28$, we have the same results for (c).

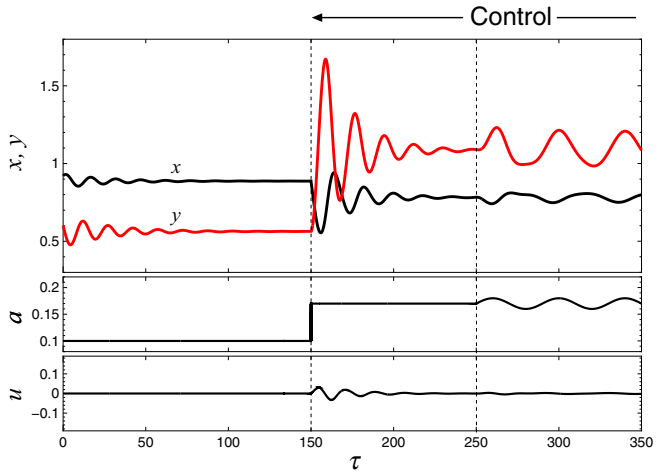

FIG. 11. (Color online) Time-series data of state variables x and y, parameter a, and control signal u for $b = 0.20$. Controller (12) with $k = 0.10$ and $T = 5.0$ is applied to system (3) at $\tau = 150$.

D. Numerical example

This subsection will report that the designed controller with $k = 0.10$ and $T = 5.0$ (see the black dot in Fig. 10) works well numerically even for a sequence of the following practical situations.

(i) Parameter a is fixed at $a = 0.10$ for time interval $\tau \in [0, 150)$ (see point B in Fig. 9).

(ii) Parameter a is changed to $a = 0.17$ at $\tau = 150$ (Fig. 9: B $\Rightarrow$ A), and then its value is fixed for $\tau \in [150, 250)$.

(iii) Parameter a is varied as $a = 0.17 + 0.01 \sin 0.05\pi(\tau - 250)$ for $\tau \geqslant 250$.

Consider situation (i). Since $\boldsymbol{p}_+$ with $a = 0.10$ is a stable focus, there is no need to use controller (12). Figure 11 shows the time series data of the state variables, parameter a, and control signal u. The trajectory of state variables x and y in the phase plane is shown in Fig. 12(a). It can be seen that

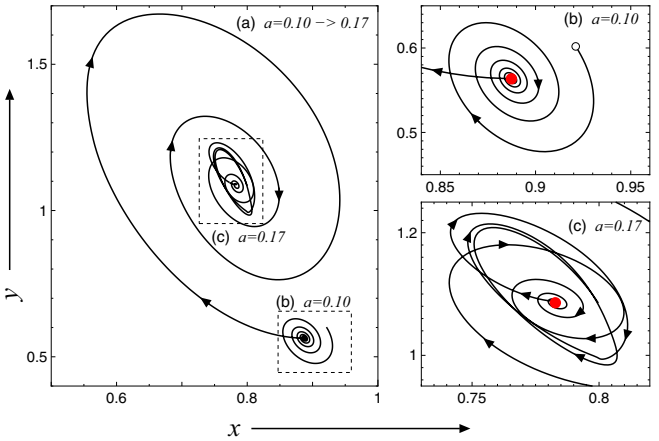

FIG. 12. (Color online) Trajectory of (x, y) on the phase plane ($b = 0.2$): (a) $a = 0.10 \to 0.17$ at $\tau = 150$, (b) $a = 0.10$, and (c) $a = 0.17 \to 0.17 + 0.01 \sin 0.05\pi(\tau - 250)$ at $\tau = 250$. Open circle: initial state $(x(0), y(0))$; red (gray) point: fixed point $\boldsymbol{p}_+$D.

the time-series data and the orbit (x,y) converge on the stable fixed point $\boldsymbol{p}_+$ [see Fig. 12(b)].

Consider situation (ii). The location of $\boldsymbol{p}_+$ jumps from the red (gray) dot in Fig. 12(b) to that in Fig. 12(c) at $\tau = 150$. At this time, the designed controller (12) is applied. The orbit (x,y) then wanders from the red (gray) dot in Fig. 12(b) to that in Fig. 12(c). Control signal u starts to oscillate at $\tau = 150$ and then converges on zero as the orbit (x,y) converges on $\boldsymbol{p}_+$. This result suggests the following two facts: The energy required for stabilization is small, and the orbit (x,y) converges exactly to $\boldsymbol{p}_+$ even if the location of $\boldsymbol{p}_+$ is unknown. These facts stem from the inherent advantages of delayed feedback control.

Consider situation (iii). Parameter a oscillates at a low frequency; the location of $\boldsymbol{p}_+$ also oscillates. From Figs. 11 and 12(c), we see that the orbit (x,y) successfully tracks the oscillating $\boldsymbol{p}_+$, even though the location of the oscillating $\boldsymbol{p}_+$ is unknown and the control signal u cannot be large. This result shows that such tracking, one of the advantages of delayed feedback control [33], is useful for the case of slow fluctuations of parameters.

V. CONCLUSION

The present paper deals with analysis and control of a dc bus system with a CPL on the basis of nonlinear science. The circuit equation describing the dc bus system, which includes five circuit parameters, is reduced to a dimensionless dynamical system with only two system parameters. The bifurcation analysis clarifies the following two scenarios for an increase of consumption power of the load: (i) for relatively small resistance, an operating point changes from a stable focus to an unstable focus via the Hopf bifurcation, changes from an unstable focus to an unstable node via a breakaway, and, finally, disappears via a saddle-node bifurcation and (ii) for a relatively large resistance, the operating point changes from a stable focus to a stable node via a breakaway and, finally, disappears via a saddle-node bifurcation. This analytical result allows us to propose a systematic procedure for designing a delayed feedback controller which can stabilize an unstable operating point. This controller has the following characteristics: the control energy required for stabilization is small due to its noninvasive property; the circuit state converges exactly on the operating point even though the location of the point is unknown; and the circuit state can track a wandering point using tiny control energy when a system parameter, such as the power consumption of the load, is slowly varied. These features demonstrate that delayed feedback control is a strong candidate for solving the destabilizing problem of dc bus systems.

It is well accepted that the destabilizing problem of dc power-grid networks needs to be solved for future practical use. Huddy and Skufca reported that delay-connection-induced amplitude death [34] can be used for this problem in a pair of dc bus systems on numerical simulations [16]. Their pioneering work is the first report on applications of nonlinear science to the destabilizing problem. In contrast, the present paper deals with a more fundamental application: bifurcation analysis and delayed feedback control of a single dc bus system. It has been reported that amplitude death can be an extension of the stabilization of a single oscillator with delayed feedback control [35]; therefore, it is expected that the fundamental results reported in the present paper will be extended to solve the destabilizing problem of dc power-grid networks by using our accumulated knowledge on amplitude death in networks [36–38].

ACKNOWLEDGMENTS

The authors thank the anonymous reviewers for their valuable comments and suggestions. This research was partially supported by JSPS KAKENHI (Grant No. 23560538).

APPENDIX: PROOF OF LEMMAS

This Appendix provides proofs of Lemmas 3 and 4.

1. Proof of Lemma 3

Consider an HP bifurcation point where the roots s of $f(s,x) = 0$ are on the imaginary axis. This situation is described by substituting $s = j\omega$, $\omega > 0$ into $f(s,x) = 0$,

$$f(j\omega,x) = b - \frac{ab}{x^2} - \omega^2 + j\omega\left(b - \frac{a}{x^2}\right) = 0. \quad \text{(A1)}$$

Elimination of a and x in $\mathrm{Re}\,[f(j\omega,x)] = 0$ and $\mathrm{Im}\,[f(j\omega,x)] = 0$ yields $\omega^2 = b(1-b)$. This equation suggests that if $b < 1$ holds, then there exists $a > 0$ such that HP bifurcation occurs at $s = \pm j\sqrt{b(1-b)}$. In contrast, if $b > 1$ holds, then HP bifurcation never occurs for any $a > 0$, due to the nonexistence of $\omega \in \boldsymbol{R}$. For $b = 1$, there exists $a > 0$ such that DZ bifurcation occurs. Thus, we see that $b < 1$ is the necessary and sufficient condition for the existence of $a > 0$ for HP bifurcation. It is easy to check that $\mathrm{Im}\,[f(j\omega,x)] = 0$ on bifurcation curve (9) holds for $x = x_+^*$ but not for $x = x_-^*$.

2. Proof of Lemma 4

At the breakaway point, $f(s,x) = 0$ has a multiplicity of roots. We have its discriminant being zero when the following holds:

$$(bx^2 + a - 2x^2\sqrt{b})(bx^2 + a + 2x^2\sqrt{b}) = 0.$$

Since $a > 0$ and $b > 0$ hold, this equation can be reduced to a simple equation,

$$a = (2\sqrt{b} - b)x^2, \quad \text{(A2)}$$

which specifies the relationship between the parameters (a, b) and x at the breakaway point. It is obvious that there exists $a > 0$ if and only if $2\sqrt{b} - b > 0$. As we are considering the stability of fixed points, x in Eq. (A2) should be the x component of $\boldsymbol{p}_\pm$. Some simple algebraic manipulation allows us to know that, for Eq. (10), Eq. (A2) with $x = x_+^*$ holds but not with $x = x_-^*$. This suggests that breakaway only occurs at $\boldsymbol{p}_+$ if Eq. (10) is satisfied. Note that we have to exclude the DZ bifurcation point, since Eq. (A2) with $x = x_+^*$ includes it.

[1] M. Rohden, A. Sorge, M. Timme, and D. Witthaut, Phys. Rev. Lett. **109**, 064101 (2012).

[2] A. Motter, S. Myers, M. Anghel, and T. Nishikawa, Nat. Phys. **9**, 191 (2013).

[3] A. Kwasinski and C. Onwuchekwa, IEEE Trans. Power Elect. **26**, 822 (2011).

[4] C. Gellins (unpublished).

[5] M. Cespedes, L. Xing, and J. Sun, IEEE Trans. Power Elect. **26**, 1832 (2011).

[6] A. Griffo, J. Wang, and D. Howe, *Proceedings of the IEEE Vehicle Power and Propulsion Conference 3-5 Sept. 2008, Harbin* (IEEE, Piscataway, NJ, 2008), pp. 1–6.

[7] P. Liutanakul, A.-B. Awan, S. Pierfederici, B. Nahid-Mobarakeh, and F. Meibody-Tabar, IEEE Trans. Power Elect. **25**, 475 (2010).

[8] X. Liu, Y. Zhou, W. Zhang, and S. Ma, IEEE Trans. Vehicular Tech. **60**, 2042 (2011).

[9] R. Gavagsaz-Ghoachani, J.-P. Martin, S. Pierfederici, B. Nahid-Mobarakeh, and B. Davat, IEEE Trans. Power Elect. **28**, 5865 (2013).

[10] M. Inoue, K. Inoue, and T. Kato, Technical Meeting on Semiconductor Power Converter, IEE Jpn. **2012**, 25 (2012).

[11] P. Magne, D. Marx, B. Nahid-Mobarakeh, and S. Pierfederici, IEEE Trans. Indust. Appl. **48**, 878 (2012).

[12] C. Onwuchekwa and A. Kwasinski, IEEE Trans. Power Elect. **25**, 2018 (2010).

[13] A. Radwan and Y.-R. Mohamed, IEEE Trans. Smart Grid **3**, 203 (2012).

[14] P. Magne, B. Nahid-Mobarakeh, and S. Pierfederici, IEEE Trans. Power Elect. **27**, 1788 (2012).

[15] E. Jamshidpour, B. Nahid-Mobarakeh, P. Poure, S. Pierfederici, F. Meibody-Tabar, and S. Saadate, IEEE Trans. Power Elect. **28**, 1833 (2013).

[16] S. Huddy and J. Skufca, IEEE Trans. Power Elect. **28**, 247 (2013).

[17] Y. Kuznetsov, *Elements of Applied Bifurcation Theory*, Applied Mathematical Sciences (Springer, Berlin, 2004).

[18] K. Pyragas, Phys. Lett. A **170**, 421 (1992).

[19] K. Pyragas, Phil. Trans. R. Soc. A **364**, 2309 (2006).

[20] R. Miyazaki, T. Naito, and J. S. Shin, SIAM J. Math. Anal. **43**, 1122 (2011).

[21] E. W. Hooton and A. Amann, Phys. Rev. Lett. **109**, 154101 (2012).

[22] A. Namajūnas, K. Pyragas, and A. Tamaševičius, Phys. Lett. A **204**, 255 (1995).

[23] H. Kokame, K. Hirata, K. Konishi, and T. Mori, Int. J. Control **74**, 537 (2001).

[24] H. Kokame, K. Hirata, K. Konishi, and T. Mori, IEEE Trans. Auto. Control **46**, 1908 (2001).

[25] H. Huijberts, W. Michiels, and H. Nijmeijer, SIAM J. Appl. Dyn. Syst. **8**, 1 (2009).

[26] A. Gjurchinovski and V. Urumov, Phys. Rev. E **81**, 016209 (2010).

[27] A. Gjurchinovski, T. Jüngling, V. Urumov, and E. Schöll, Phys. Rev. E **88**, 032912 (2013).

[28] The delayed feedback control has the noninvasive property because the control signal vanishes whenever the system state is on the fixed point.

[29] R. Dorf and R. Bishop, *Modern Control Systems* (Prentice-Hall, New Jersey, 2010).

[30] A. Dhooge, W. Govaerts, Y. A. Kuznetsov, H. G. Meijer, and B. Sautois, Math. Comput. Model Dyn. Syst. **14**, 147 (2008).

[31] Since it is difficult to derive α and ω branches analytically, we numerically estimate them by the software PPLANE [39].

[32] If the characteristic function of an unstable fixed point without control has an odd number of positive real roots, then the fixed point will never be stabilized by delayed feedback control [23,24,40].

[33] S. Bielawski, D. Derozier, and P. Glorieux, Phys. Rev. A **47**, R2492 (1993).

[34] This phenomenon is the stabilization of an unstable fixed point in oscillators coupled by time-delay diffusive connections [41,42,43].

[35] K. Konishi, Phys. Rev. E **70**, 066201 (2004).

[36] K. Konishi, Phys. Lett. A **341**, 401 (2005).

[37] K. Konishi, H. Kokame, and N. Hara, Phys. Rev. E **81**, 016201 (2010).

[38] L. B. Le, K. Konishi, and N. Hara, Phys. Rev. E **87**, 042908 (2013).

[39] J. C. Polking and D. Arnold, *Ordinary Differential Equations Using MATLAB* (Prentice-Hall, New Jersey, 2004).

[40] T. Ushio, IEEE Trans. Circuits Syst. I **43**, 815 (1996).

[41] D. Reddy, A. Sen, and G. Johnston, Physica D **129**, 15 (1999).

[42] G. Saxena, A. Prasad, and R. Ramaswamy, Phys. Rep. **521**, 205 (2012).

[43] A. Koseska, E. Volkov, and J. Kurths, Phys. Rep. **531**, 173 (2013).